

Hairpin DNA Functionalized Gold Nanorods for mRNA Detection in Homogenous Solution

Guoke Wei,^{a, b} Jun Yu,^c Jinliang Wang,^b Peng Gu,^a David J. S. Birch,^a and Yu Chen^{a,*}

^a Photophysics Group, Centre for Molecular Nanometrology, Department of Physics, SUPA, University of Strathclyde, John Anderson Building, 107 Rottenrow, Glasgow G4 0NG, UK

^b Department of Physics, Beihang University, Beijing 100191, China

^c Strathclyde Institute of Pharmacy and Biomedical Sciences, Royal College, University of Strathclyde, 204 George Street, Glasgow G1 1XW, UK

ABSTRACT: We report a novel fluorescent probe for mRNA detection. It consists of a gold nanorod (GNR) functionalized with fluorophore labeled hairpin oligonucleotides (hpDNA) that are complementary to the mRNA of a target gene. This nanoprobe was found to be sensitive to a complementary oligonucleotide, as indicated by significant changes in both fluorescence intensity and lifetime. The influence of the surface density of hpDNA on the performance of this nanoprobe was investigated, suggesting that high hybridization efficiency could be achieved at a relatively low surface loading density of hpDNA. However, steady-state fluorescence spectroscopy revealed better overall performance, in terms of sensitivity and detection range, for nanoprobe with higher hairpin coverage. Time-resolved fluorescence lifetime spectroscopy revealed significant lifetime changes of the fluorophore upon hybridization of hpDNA with targets, providing further insight on the hybridization kinetics of the probe as well as the quenching efficiency of GNRs.

KEYWORDS: gold nanorods, hairpin DNA, mRNA detections, fluorescence lifetime

* Corresponding author, Email: y.chen@strath.ac.uk

1. Introduction

Messenger RNA (mRNA) plays a key role in the cellular production of protein. Detection of mRNA biomarkers with good specificity and sensitivity will enable an early-stage diagnosis of disease such as cancer and assist in monitoring and evaluating the efficacy of treatment. Moreover, detection of mRNA provides valuable information for understanding the fundamental metabolism of cells.^{1,2} For this purpose, a number of techniques have been developed.³ Among them, nucleic acids-based detection and quantification methods have attracted substantial interest since nucleic acids possess the inherent property to selectively bind to the complementary targets through Watson-Crick base-pairing. One of the promising approach to detect mRNA, often denoted as molecular beacon (MB), is a hairpin-shaped oligonucleotide with a fluorophore-quencher pair that undergoes a spontaneous fluorogenic conformational change upon

37 hybridization with the complementary nucleic acid target.^{4,5} It offers great opportunities in
38 homogeneous assay of mRNA and also the capability of real-time monitoring of the expression
39 of mRNAs in living cells, even down to single-cell level, resulting from its high sensitivity and
40 enhanced specificity.⁶⁻⁹

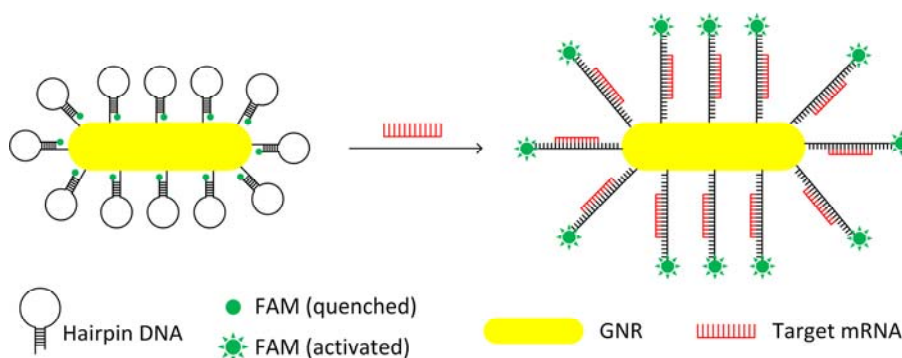
41 However, the traditional MB suffers from problems of lacking universal organic quenchers¹⁰
42 and requiring transfection reagents for cellular internalization.⁸ Recent studies show that these
43 limitations can be elegantly addressed by gold nanoparticles (AuNP). It has been proven that
44 AuNP are highly efficient quenchers for a range of organic fluorophores¹⁰⁻¹³ and exhibit long-
45 range fluorescence quenching capability.¹⁴ Moreover, Au nanospheres (AuNS) functionalized by
46 oligonucleotides display several fascinating features. For example, highly efficient cellular
47 uptake without the need of transfection reagents, extraordinary intracellular stability against
48 enzymatic degradation and enhanced binding capability of complementary nucleic acids.¹⁵⁻¹⁷
49 Additionally, AuNP are biocompatible and have versatile surface modifications especially
50 through the well-established gold-thiol chemistry. By taking the advantages of AuNP and MB, a
51 novel nanoprobe has been developed recently, in which AuNS were covalently functionalized by
52 hairpin oligonucleotides dually labeled with fluorophore and thiol.¹⁸ This nanoprobe shows
53 promising applications in simultaneous multianalysis of nucleic acid with high sensitivity and
54 specificity.¹⁸⁻²⁰ More importantly, spatial-temporal information about nucleic acid targets in
55 living cells can be acquired by using this AuNP-MB conjugate as intracellular probe since the
56 fluorophores are still anchored to the AuNP rather than being released into the cytoplasm when
57 binding to the targets.^{21,22}

58 Compared to AuNS, gold nanorods (GNR) exhibit excellent shape-dependent optical
59 properties. By varying the aspect ratio, the longitudinal plasmon band of GNR can be finely

60 tuned from visible to near-infrared regions.^{23,24} This is of particular interest for biological
61 applications due to the high transmission of tissues in the near-infrared window (650-900 nm).²⁵
62 In addition to the large absorption and scattering cross section, GNR have strong two-photon
63 luminescence arising from the localized surface plasmon resonance.²⁶⁻²⁸ Two-photon excitation
64 holds promise for intracellular studies as it has higher spatial resolution, deeper penetration and
65 less photo-damage compared to single-photon excitation. Interestingly, two-photon luminescence
66 from GNR shows a characteristic short lifetime (<100 ps) distinguishable from many organic
67 dyes and autofluorescence, offering benefit in fluorescence lifetime imaging microscopy
68 (FLIM).²⁹ These unique features make GNR promising candidates for numerous biological and
69 biomedical applications, including biological imaging,³⁰ gene/drug delivery,³¹ and photothermal
70 therapy.³²

71 Considering the unique properties of GNR, it is expected that GNR coupled with hairpin
72 oligonucleotides will offer great opportunity in mRNA detection and imaging. Recently we have
73 reported a new RNA nanoprobe based on functionalized GNR and the influence of hairpin
74 structure on the quenching efficiency of the energy transfer pair of GNR and Cy5.³³ Due to the
75 steric structure of hpDNA and difficulty in completely replacing CTAB bilayer surrounding
76 GNRs with biomolecules, the functionalization of GNRs with hpDNA have been found
77 challenging and less reported. Here, to the best of our knowledge, we report for the first time the
78 functionalization of GNR with 6-carboxyfluorescein (FAM) labeled hairpin DNA (hpDNA)
79 (Scheme 1), and influence of the synthesis condition on the performance of this nanoprobe in
80 target mRNA detection using both steady-state and time-resolved fluorescence spectroscopies.
81 FAM was chosen as it can be attached to the 3' end and allows reliable attachment of
82 oligonucleotide with thiol molecule modified in the 5' end. Our results show that the GNR-

83 hpDNA conjugates are highly sensitive probes for mRNA detection with high signal-to-
84 background ratio. Moreover, we investigated the influence of the surface density of hpDNA on
85 GNR on the performance of this nanoprobe and found that high hybridization efficiency could be
86 achieved at relatively low surface loading density of hpDNA. The fluorescence lifetime
87 measurements revealed the recovery of fluorescence lifetime in the hybridization events,
88 indicating the conformational change of hpDNA when binding to target mRNA complement.
89 Significantly, fluorescence lifetime spectroscopy is demonstrated as a powerful tool for
90 fluorescence-based mRNA detection.



Scheme 1. Schematic illustration of hairpin DNA functionalized GNR for mRNA detection.

94 3. Experimental section

95 3.1 Materials

96 All chemicals were purchased from Sigma-Aldrich and used as received. All buffers were
97 prepared using nuclease-free water obtained from Sigma-Aldrich. Thiolated oligonucleotides and
98 the corresponding complementary oligonucleotides were purchased from Eurofins MWG Operon
99 and Integrated DNA Technologies, respectively.

100 3.2 Synthesis of Gold Nanorods

101 Gold nanorods were synthesized according to the silver-assisted seed-mediated growth
102 method.^{34,35} Briefly, 2.5 mL of 0.001 M HAuCl₄ was mixed with 7.5 mL of 0.2 M
103 Hexadecyltrimethylammonium bromid (CTAB) solution. Next, 0.6 mL of freshly prepared ice-
104 cold 0.01 M NaBH₄ was quickly added to the solution under vigorous stirring, forming a
105 brownish-yellow seed solution. The seed solution was vigorously stirred for another 2 min and
106 then kept undisturbed at room temperature for 3 h before used. To make growth solution, 200
107 mL of 0.2 M CTAB solution was gently mixed with the following solutions in the following
108 order: 200 mL of 0.001 M HauCl₄, 8 mL of 0.004 M AgNO₃, 2.8 mL of 0.0778 M ascorbic acid.
109 Then, 0.4 mL of the colloidal gold seeds was added to the growth solution and the reaction
110 mixture was left on the bench undisturbed overnight. The obtained nanorods were spun down by
111 centrifugation (14500 rpm, 12 min) and finally re-suspended in 2 mL of distilled water. This
112 process produced gold nanorods of diameter 12.7 ± 1.8 nm and length 51.6 ± 8.2 nm as derived
113 from TEM analysis (Figure 1(a)), and longitudinal surface plasmon resonance peak centered at
114 800 nm. Experimentally, reproducibility of further functionalization was ensured by producing
115 nanorods of similar surface plasmon resonance property.

116 *3.3 Ligand Exchange of Nanorods*

117 The CTAB surfactant on the GNR surface was replaced with mercaptohexanoic acid (MHA)
118 using a round-trip phase transfer ligand exchange approach.³⁶ Firstly, the CTAB coated GNRs
119 (NR-CTAB) were extracted from the aqueous phase to the organic phase by dodecanethiol
120 (DDT) upon the addition of acetone following a few second swirling. During this process, the
121 CTAB was displaced by DDT, resulting in DDT coated GNR (NR-DDT). The volume ratio of
122 the concentrated NR-CTAB solution, DDT and acetone was 1:1:4. The excess DDT was then
123 diluted by adding an aliquot of toluene and five aliquots of methanol and washed away by

124 centrifugation (5000 rpm, 8 min). The NR-DDT were re-suspended in 1 mL toluene by brief
125 sonication. Next, the GNR were extracted back to the aqueous phase using MHA as the
126 exchanged ligand. The NR-DDT were added to 9 mL of 0.01 M MHA in toluene at ~90 °C and
127 vigorously stirred. Reflux and stirring continued until visible aggregation was observed (within
128 ~15 min), indicating that MHA has replaced the DDT. The MHA coated GNR (NR-MHA) were
129 then left to sediment, washed twice with aliquots of toluene via decantation and once with an
130 aliquot of isopropanol to remove all reaction byproducts and excess MHA. Finally, the NR-
131 MHA were re-suspended in 1×Tris-borate-EDTA (TBE) buffer (pH 8.3) with a high
132 concentration of ~100 nM. The GNR concentrations were determined by optical absorption
133 using the reported extinction coefficients.³⁷

134 *3.4 Hairpin DNA Functionalization of Nanorods*

135 A thiolated hairpin DNA (hpDNA) with a 6-carboxyfluorescein (FAM) label in the 3' end (5'-
136 HS-(CH₂)₆-TTTTT GCGAG TTG GTG AAG CTA ACG TTG AGG CTCGC-FAM-3'); the
137 underlined bases represent the stem sequence) was designed to recognize a 21-nucleotide region
138 of c-myc mRNA. A 5-base polythymine spacer was inserted following the 5' thiol in order to
139 reduce self-adsorption of DNA to the surface of GNR.^{38,39} The disulfide bonds of thiolated
140 hpDNA were reduced by tris(2-carboxyethyl)phosphine hydrochloride (TCEP) in 1×TE buffer
141 (pH 8.0) with TCEP/DNA molar ratio of 100:1. After 60-min incubation at room temperature
142 while shaking, the activated DNA was precipitated from the mixture by sodium acetate and
143 ethanol. Specifically, to the reduced DNA solution, appropriate quantities of 3 M sodium acetate
144 and 100% ethanol were added so that the final salt concentration was 0.3 M and the final ethanol
145 concentration was 70%. The mixture was incubated 20 min at -20 °C and then spun for 5 min at

146 13000 rpm. The supernatant was discarded and the pellet was re-suspended in 1×TE buffer (pH
147 8.0).

148 The NR-MHA were conjugated with hpDNA by a salt aging process.^{40,41} The hpDNA of
149 different concentrations (5.0, 3.5, 2.0, 1.0, 0.5 μM) were incubated with 5 nM NR-MHA,
150 respectively, in 10 mM phosphate buffer (pH 7.0) with 0.02 (wt/vol) % SDS at room
151 temperature. After 3-hour incubation, 10 μL of salting solution containing 500 mM NaCl, and
152 0.02% sodium dodecyl sulfate (SDS) in 10 mM phosphate buffer (pH 7.0) was added to the
153 mixture every 60 min. This step was repeated for a total of five times to reach a final NaCl
154 concentration of 100 mM. The salted sample was further incubated at room temperature for 16
155 hours. The NR-hpDNA conjugates were purified of excess reagents via centrifugation at 13000
156 rpm for 15 min at 4 °C. The precipitate was washed four times with washing buffer (10 mM
157 Phosphate buffer + 0.02% SDS, pH 7.5), and an additional three times with 10 mM phosphate
158 buffer (pH 7.5) by repetitive centrifugation and dispersion, which was finally re-suspended in 10
159 mM phosphate buffer (pH 7.5) and stored at 4 °C.

160 *3.5 Quantitation of Hairpin DNA Loading on Nanorods*

161 The hpDNA loaded on GNR was quantified by chemical displacement and fluorescence
162 spectroscopy.³⁸ The purified NR-hpDNA conjugates were incubated in 20 mM mercaptoethanol
163 (ME) overnight with shaking at room temperature, displacing the hpDNA from GNR. The
164 released hpDNAs were then separated from GNR via centrifugation (13500 rpm, 15 min). The
165 fluorescence of the displaced hpDNA was measured and converted to molar concentration of
166 hpDNA by interpolation from a standard linear calibration curve, which was prepared with
167 known concentrations of fluorophore-labeled hpDNA with identical buffer pH, ionic strength,

168 and ME concentration. The average number of hpDNA per GNR was obtained by dividing the
169 molar concentration of hpDNA by the original GNR concentration.

170 *3.6 Hybridization Efficiency of NR-hpDNA probes*

171 Hybridization efficiency was quantified according to the published protocol.³⁸ TAMRA-labeled
172 complementary DNA (TMR-cDNA) were incubated with NR-hpDNA under hybridization
173 conditions (3 μ M TMR-cDNA, 10 mM phosphate buffer with 100 mM NaCl, pH 7.5, 24 h).
174 Nonhybridized cDNA-TMR were removed and rinsed three times by 10 mM phosphate buffer
175 (pH 7.5) through centrifugation (13500 rpm, 15 min). After that, the TMR-cDNAs were
176 dehybridized by addition of NaOH (final concentration 50 mM, pH 11-12, 2 h). The
177 dehybridized TMR-cDNAs were then separated from the mixture by centrifugation, and
178 neutralized by addition of 1 M HCl. The concentration of dehybridized TMR-cDNA and the
179 corresponding hybridization efficiency were determined by fluorescence spectroscopy analysis.

180 *3.7 Hybridization Kinetics*

181 The complementary DNA (cDNA) was used to investigate the hybridization kinetics of the
182 nanoprobe. The hybridization experiments were carried out in the hybridization buffer (10 mM
183 phosphate buffer of pH 7.5, 100 mM NaCl) containing 0.22 nM nanoprobe and 880 nM cDNA.
184 The excitation and emission wavelengths were 490 nm and 517 nm for fluorescein, respectively.

185 *3.8 Sensitivity Experiment*

186 The nanoprobe (0.22 nM) were incubated with varying concentrations of cDNA (0, 1, 5, 10, 20,
187 30, 40, 50, 80, 100, 200, and 300 nM) in the hybridization buffer for 2 hours at 37 °C before
188 measuring the fluorescence recovery.

189 *3.9 Fluorescence Lifetime Measurements*

190 Time-resolved fluorescence measurements were performed using the time-correlated single-
 191 photon counting (TCSPC) technique on an IBH Fluorocube fluorescence lifetime system (Horiba
 192 Jobin Yvon IBH Ltd., Glasgow, UK) equipped with both excitation and emission
 193 monochromators. A pulsed light-emitting diode (LED) of 474 nm operating at 1 MHz repetition
 194 rate was used as the excitation source. A longpass filter of 505 nm was used to minimize the
 195 detection of excitation light. Fluorescence decays were measured at the magic angle (54.7°) to
 196 eliminate polarization artifacts. Data analysis was performed using nonlinear least squares with
 197 the IBH iterative reconvolution software (DAS6 data analysis package). The fluorescence
 198 intensity decays were analyzed in terms of the multi-exponential model as the sum of individual
 199 single exponential decays:

$$200 \quad I(t) = \sum_i \alpha_i \exp\left(-\frac{t}{\tau_i}\right), \quad (1)$$

201 where τ_i are the decay times and α_i the associated amplitudes. The fractional contribution of
 202 each lifetime component to the steady-state intensity is represented by

$$203 \quad f_i = \alpha_i \tau_i / \sum_k \alpha_k \tau_k . \quad (2)$$

204 The average lifetime ($\bar{\tau}$) is calculated as

$$205 \quad \bar{\tau} = \sum_i f_i \tau_i . \quad (3)$$

206 As noted, a very short lifetime component (less than 100 ps) was found in both cases before
 207 and after hybridization. This lifetime is below the system response time limit and is attributed to
 208 the scattering of GNR. This was excluded in the multi-exponential fittings by deliberately fixing
 209 one of the lifetime components at a value of 0.5 channels.

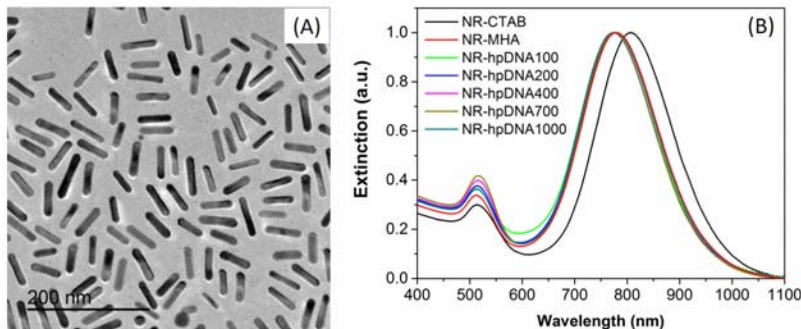
210 To retrieve the lifetime distributions, a model-free maximum entropy method (MEM) was
 211 used, using the software Pulse 5 (MaxEnt Ltd, Cambridge, UK).⁴² It provides an unique solution

212 to fluorescence lifetime data using a broad window of decay terms fit by simultaneous
213 minimization of the χ^2 and maximization of a statistical entropy function. The lifetime
214 distribution $h(\tau)$ is related to the fluorescence intensity decay $I(t)$ by

$$215 \quad I(t) = \int_0^{\infty} h(\tau) \exp\left(-\frac{t}{\tau}\right) d\tau. \quad (4)$$

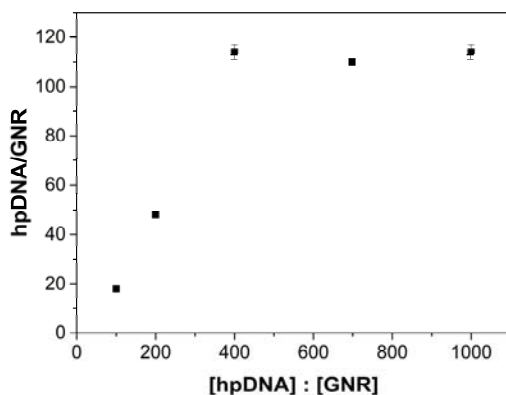
216 **3. Results and Discussion**

217 The bilayer CTAB on the surface of as-made GNR may not only cause cytotoxic effect to living
218 cells,^{43,44} but also can be problematic for further surface modification with bioconjugates.²³ Thus,
219 the CTAB layers were replaced with MHA prior to conjugation with hpDNA, using a round-trip
220 phase transfer ligand exchange approach.³⁶ As shown in Figure 1(b), the longitudinal surface
221 plasmon resonance (LSPR) of the CTAB-coated GNR was centered at 807 nm. This LSPR band
222 was blue-shifted to 780 nm without significant broadening after the ligand exchange process,
223 indicating a successful ligand exchange without apparent aggregation. The hpDNA were
224 conjugated with GNR via a salt-aging process,^{40,41} in which different molar ratios of hpDNA to
225 GNR, namely 100:1, 200:1, 400:1, 700:1 and 1000:1, were used. The UV-vis spectra showed
226 that the LSPR bands of all hpDNA-functionalized GNRs did not exhibit significant change
227 compared to that of MHA modified GNR (NR-MHA), regardless of different molar ratios of
228 hpDNA to GNR used in the synthesis process (Figure 1(b)). This was possibly due to
229 centrifugation processes where a fraction of GNRs with high aspect ratios were inevitably left in
230 the supernatant after each round of centrifugation as the sedimentation velocity was dictated by
231 the hydrodynamic behavior of nanoparticles,⁴⁵ making it difficult to observe the slight changes of
232 LSPR peaks among GNR-MHA with different hpDNA coverages experimentally.



233
 234 **Figure 1.** (a) TEM image of the gold nanorods. The scale bar is 200 nm; (b) Extinction spectra
 235 of GNR made with CTAB and GNRs with surface modifications of MHA and hpDNA-FAM.
 236 The NR-CTAB was suspended in distilled water, while NR-MHA and NR-hpDNA-FAM were
 237 suspended in 1×TBE (pH 8.3) and 10 mM phosphate buffer (pH 7.5), respectively.

238 To quantify the average number of hpDNA assembled on a GNR, hpDNA on GNRs were
 239 released by mercaptoethanol (ME) and the concentration of hpDNA was determined by
 240 fluorescence intensity against a standard correlation curve between fluorescence intensity and
 241 hpDNA-FAM concentration.³⁸ The surface packing density of hpDNA on single GNR was
 242 obtained with known GNR particle density. As depicted in Figure 2, the surface loading of
 243 hpDNA on GNR varies with the molar ratio of hpDNA to GNR in the mixture. It is interesting to
 244 note that the surface loading of hpDNA reached a maximum of ~114 at a molar ratio of 400:1,
 245 and maintained at this value even with higher molar ratios. This is well below the value of
 246 maximum loading, ~168 oligonucleotides per GNR, as predicted by Hill's model.⁴⁶ In the
 247 successive study, samples made from molar ratios of 100:1, 200:1 and 400:1 were investigated,
 248 denoted as NR-hpDNA100, NR-hpDNA200 and NR-hpDNA400, respectively. The footprints of
 249 hpDNA loading on GNR were calculated to be approximately 114.4, 42.9 and 18.1 nm² for NR-
 250 hpDNA100, NR-hpDNA200 and NR-hpDNA400, respectively.

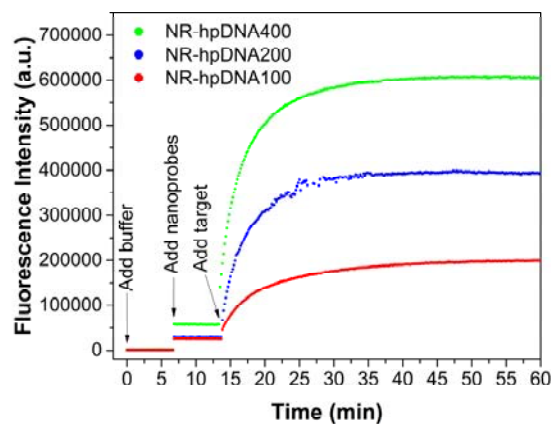


251
 252 **Figure 2.** A correlation between surface loading of hpDNA on each GNR and molar ratio of
 253 hpDNA to GNR in the synthesis process. Error bars are one standard deviation from three
 254 measurements.

255
 256 To test the performance of the nanoprobe, we first examined their fluorogenic responses to
 257 the addition of targets. The nanoprobe was exposed to an excess amount of perfectly matched
 258 complementary DNA (cDNA) (880 nM). As demonstrated by the kinetic measurements in
 259 Figure 3, all of the nanoprobe showed an instant fluorescence recovery upon adding cDNA, and
 260 the fluorescence intensities reached saturation levels in short time periods. This is consistent with
 261 the previous studies using MB and AuNS-MB conjugates,^{5,18,47} indicating that the GNR-based
 262 nanoprobe retained the advantage of MB. In addition, it is noted that the surface packing density
 263 of hpDNA had a great impact on the hybridization kinetics of nanoprobe. It is apparent from
 264 Figure 3 that nanoprobe with higher surface coverage of hpDNA displayed higher target-capture
 265 rate. The hybridization rates could be quantitatively obtained as the first-ordered differentiation
 266 of the curve in Figure 3. It was found that, in the initial rapid hybridization period upon target
 267 addition, the response of NR-hpDNA400 to cDNA was about 1.4 and 5.3 times faster than that
 268 of NR-hpDNA200 and NR-hpDNA100, respectively. The fluorescence intensities of NR-

269 hpDNA400 and NR-hpDNA200 reached saturation levels in a similar time period, while a longer
270 time was needed for NR-hpDNA100.

271 As also shown in Figure 3, the fluorescence intensity of FAM in the absence of target strands,
272 i.e. background signal, was low but measurable for all three nanoprobe. The background signal
273 of NR-hpDNA400 was relatively higher than that of NR-hpDNA200, while the latter was just
274 slightly higher than that of NR-hpDNA100. The saturation fluorescence signal in the presence of
275 targets, on the other hand, was found to have a positive relationship with hpDNA loading. In
276 addition to fluorescence intensity, which is primarily related to the number of open hpDNA,
277 another factor usually used to determine the sensor performance of molecular beacon is the
278 quenching efficiency, defined as $(1-F_{\text{closed}}/F_{\text{open}})\times 100\%$, where F_{closed} and F_{open} are the
279 fluorescence intensity of nanoprobe in the absence of target and its stable level in the presence of
280 excess target, respectively. For NR-hpDNA400, NR-hpDNA200 and NR-hpDNA100, the
281 quenching efficiencies were calculated to be 90.8%, 93.3% and 88.1%, respectively, indicating a
282 similar and good quenching effect of all three nanoprobe.



283
284 **Figure 3.** Kinetic fluorescence measurements of the nanoprobe upon hybridization. The
285 concentrations of NR-hpDNA and cDNA were 0.22 and 880 nM, respectively. Excitation
286 wavelength: 490 nm; fluorescence wavelength: 517 nm.

287

288 **Table 1.** Hybridization efficiency of NR-hpDNA nanoprobe with different probe surface
289 packing densities.

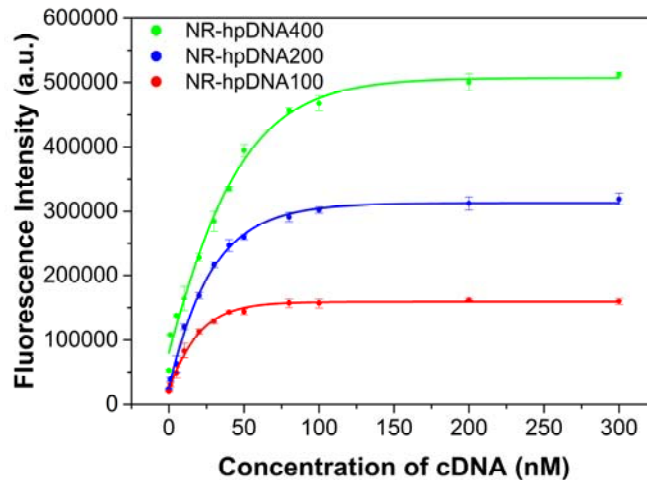
Samples	Surface coverage (hpDNA/cm ²)	Hybridized coverage (hpDNA/cm ²)	Hybridization efficiency
NR-hpDNA400	$(5.54 \pm 0.13) \times 10^{12}$	$(1.51 \pm 0.01) \times 10^{12}$	27.19 %
NR-hpDNA200	$(2.33 \pm 0.05) \times 10^{12}$	$(1.21 \pm 0.05) \times 10^{12}$	52.08 %
NR-hpDNA100	$(0.87 \pm 0.07) \times 10^{12}$	$(0.83 \pm 0.07) \times 10^{12}$	94.44 %

290

291 To further evaluate the effectiveness of the NR-hpDNA nanoprobe for nucleic acid detection,
292 the average number of target strands hybridized with hpDNA on each nanoprobe was quantified
293 using the protocol reported by Demers *et al.*³⁸ An excess of TMR-cDNA (3 μM as final
294 concentration) was incubated with NR-hpDNA nanoprobe in the hybridization buffer for 24 h to
295 maximize the hybridizations. The influence of TMR labels on the hybridization (duplex
296 formation) is negligible.⁴⁸ Following a centrifuge process to remove unbound excess TMR-
297 cDNA, the hybridized TMR-cDNA were released by denaturing the duplex DNA and separated
298 from the NR-hpDNA nanoprobe. The concentration of dehybridized TMR-cDNA was deduced
299 from its fluorescence intensity according to a concentration-intensity correlation curve. Table 1
300 lists the surface coverage of hairpins, surface coverage of hybridized hairpins (with TMR-
301 cDNA) and hybridization efficiency of three NR-hpDNA nanoprobe. Interestingly, the number
302 of captured target strands increased with increasing surface coverage of hpDNA on GNR, which
303 is consistent with the saturate fluorescence intensity observed in the kinetic studies (Figure 3).
304 However, the hybridization ratio decreased from 94.44 % to 27.19 % as the hpDNA packing
305 density increased from 0.87×10^{12} to 5.54×10^{12} hpDNA/cm². This indicates that a higher hairpin

306 density results in an increased total target binding, but a relatively lower efficiency in
307 hybridizing hpDNA available on GNR.^{49,50} This is not surprising as previous studies have found
308 that, for both DNA on thin films and nanoparticles, the efficiency of DNA hybridization is
309 governed by both the electrostatic repulsion between neighboring DNA strands and the steric
310 hindrance between tethered DNA probes.^{38,49,51} An upright conformation of oligonucleotide, that
311 is preferred for hpDNA of relatively high surface coverage due to the repulsive force between
312 neighboring oligonucleotides, is favorable for hybridizations. On the other hand, densely packed
313 oligonucleotide monolayers would reduce accessibility of incoming target strands.

314 Figure 4 depicts the correlation between fluorescence intensity of nanoprobe and the target
315 concentration. As expected, for all nanoprobe, the recovery of the fluorescence signal was
316 positively correlated to the target concentration. Apparent changes in the fluorescence intensities
317 were observed at a target concentration of 1 nM. As the concentration of cDNA increased, the
318 fluorescence intensity increased monotonically until saturated at a stable plateau at relatively
319 high target concentration. These again indicated the opening of hairpin structure upon
320 hybridization. Significantly, nanoprobe of higher hairpin coverage not only showed stronger
321 fluorescence intensity at the same target concentration, but also a higher saturation signal at a
322 larger target saturation concentration. This means that the nanoprobe of higher hairpin coverage
323 had better sensitivity and larger detection range. The limit of detection of probe NR-hpDNA400
324 (LOD=3.3×standard deviation of the response/the slope of the calibration curve up to 50nM) was
325 found to be 0.68 nM.



326
 327 **Figure 4.** Dose response of the nanoprobes (0.22 nM) with different surface packing densities of
 328 hpDNA. The concentrations of perfectly complementary DNA were 0, 1, 5, 10, 20, 30, 40, 50,
 329 80, 100, 200 and 300 nM. Excitation wavelength: 485 nm; emission peak: 517 nm.

330
 331 Furthermore, time-resolved fluorescence spectroscopy was employed to evaluate the lifetime
 332 change of FAM on the nanoprobes before and after hybridized with targets. For comparison, the
 333 fluorescence intensity decay of free hpDNA-FAM was analysed prior to conjugation to GNR.
 334 Two lifetime components were found to present in the free hpDNA-FAM sample, where the long
 335 lifetime of 3.92 ns was the dominant one, accounting for a fractional contribution of 98%. It is
 336 worth noting that the fluorescence decay of free hpDNA-FAM in “closed” state (without binding
 337 to cDNA) was slightly different from that in “open” state (hybridized with cDNA) with both
 338 long and short lifetimes of free open-state hpDNA-FAM slightly greater than those of hpDNA-
 339 FAM in “closed” state, as determined from multi-exponential analysis (Table 2). This is
 340 probably due to the close proximity of FAM to the guanine in the hairpin conformation. Previous
 341 studies found that the fluorescence of FAM could be quenched by guanosine nucleotide due to

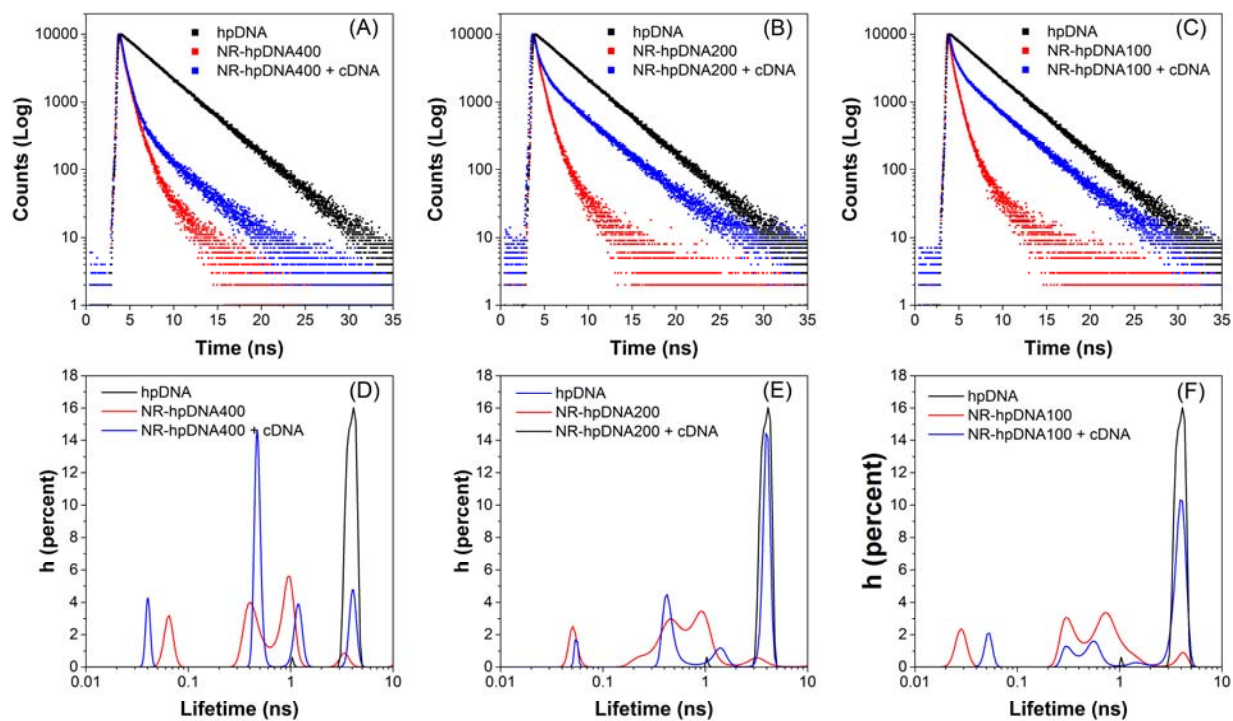
342 the photoinduced electron transfer.⁵²⁻⁵⁴ Indeed, the hpDNA-FAM hybridized with cDNA showed
343 a 1.7-fold increase in fluorescence intensity with respect to the hpDNA-FAM in “closed” state.

344 After being assembled on GNRs, the FAM molecules were held to the close proximity of
345 GNR surfaces by the hairpin DNA structure in the absence of targets. Consequently, the
346 fluorescence lifetime of FAM was dramatically shortened, due to the fluorescence quenching
347 effect induced by GNR. Multi-exponential fitting shows that the FAM in NR-hpDNA400 has
348 three lifetime components of 2.87 ns (8%), 0.85 ns (59%) and 0.35 ns (33%) (Table 2). As noted,
349 the shorter lifetime components of less than 1 ns were dominant in the fluorescence decay. The
350 total average lifetime was calculated to be 0.85 ns, about 4.5-fold smaller than that of the free
351 closed-state hpDNA-FAM, confirming the quenching effect introduced by GNR. Upon target
352 binding, the fluorescence lifetime of FAM recovered as expected, with three lifetime components
353 of 3.93 ns (23%), 1.05 ns (24%) and 0.45 ns (53%) (Table 2). The average lifetime was 1.40 ns,
354 about 1.6-fold increase compared to that of the closed-state nanoprobe. All of the lifetime
355 components increased with the longest one approaching that of free open-state hpDNA-FAM.
356 The fractional contribution of the longest lifetime component significantly increased, whereas
357 the fractional contribution of shorter components decreased. The existence of short lifetime
358 components indicated that not all hpDNA opened, in line with previous finding that about 27%
359 of hpDNA were in open states. The fluorescence lifetime distributions retrieved from maximum
360 entropy method (MEM) are shown in Figure 5 (D). By summing the area under the peaks, the
361 fractional contributions for a continuous lifetime distribution can be determined. The MEM
362 analysis reveals that the lifetime spectrum of NR-hpDNA400 in the absence of cDNA consists of
363 three peaks located at 3.37 ns (22%), 0.93 ns (52%) and 0.44 ns (22%) and one extremely small
364 distribution centred at 0.06 ns (1%). Significantly, upon hybridization to cDNA, the 3.37-ns

365 lifetime component shifted towards a greater value (4.06 ns) with the fractional contribution
366 increasing to 63%, whereas the 0.93-ns band shifted to 1.18 ns with the fractional contribution
367 falling to 17%. Meanwhile, the second shortest lifetime peak became relatively sharp and narrow
368 with barycentre at 0.48 ns and fractional contribution of 20%. In contrast, the contribution from
369 the shortest lifetime peak (0.04 ns) almost vanished in the fluorescence decay, only accounting
370 for a fractional contribution of 0.37%. The average lifetimes of NR-hpDNA400 before and after
371 hybridizations were calculated to be 1.6 ns and 2.9 ns, respectively. Due to the complexity of
372 fluorescence decay in the NR-hpDNA-FAM system, it is not surprising that there are
373 discrepancies between the fitting results obtained from MEM and multi-exponential models.
374 Nevertheless, the MEM analysis is qualitatively consistent with the multi-exponential analysis.
375 The kinetics revealed by the fluorescence lifetime measurements are in accordance with the
376 observations obtained by steady-state fluorescence spectroscopy (Figure 3).

377 Comparing the closed-state nanoprobe with different hpDNA densities, multi-exponential
378 analysis showed similar average lifetimes of ~ 0.8 ns (Table 2), suggesting a similar hairpin
379 configuration for all three nanoprobe. However, the change of average lifetime upon
380 hybridization was found to be dependent on the hpDNA density. After binding to targets, three
381 lifetime components were found similar for all three nanoprobe (Table 2). However, the
382 corresponding fractional contributions of similar lifetime component were different. As the
383 surface density of hpDNA decreased, the fractional contribution of the longest lifetime
384 component (~ 3.95 ns) increased and became dominant in the fluorescence decay, while the
385 fractional contributions of the shorter lifetime components decreased. The average lifetimes of
386 NR-hpDNA400, NR-hpDNA200 and NR-hpDNA100 after binding to targets were 1.40, 2.71
387 and 3.02 ns, respectively. As shown in Figure 5 (E and F), the lifetime spectra retrieved from

388 MEM clearly demonstrate that the longest lifetime distribution centered at ~ 4 ns played an
389 essential role in the decay of the hybridized nanoprobe, while the relatively broad lifetime
390 distribution ranging from 0.2 – 1.5 ns was predominant in the non-hybridized samples. Moreover,
391 the MEM analysis shows that the average lifetimes of NR-hpDNA-400, NR-hpDNA200 and
392 NR-hpDNA100 were ~ 1.6 ns before hybridization, but increased to 2.9, 3.7 and 3.8 ns,
393 respectively, after exposure to an excess of target strands. These were again in agreement with
394 the multi-exponential analysis results. The changes in average lifetime revealed by both fitting
395 methods were in line with hybridization efficiency found in Table 1. However, the average
396 lifetime for NR-hpDNA100 after hybridization was still smaller than that of free hybridized
397 DNAs, although 94% of hpDNA were hybridized as revealed above. This is possibly because
398 that not all hybridized hpDNAs fully stretched out from the GNR surface, due to low hpDNA
399 packing density and lacking of electrostatic repulsions from the neighbors. This indicates that
400 time-resolved fluorescence spectroscopy is a powerful technique not only for providing
401 information related to hairpin conformational changes, as demonstrated recently,⁵⁵ but also to
402 hybridization ratio of assembled hpDNAs.



403
 404 **Figure 5.** (Upper panel) Fluorescence intensity decay curves of (A) NR-hpDNA400, (B) NR-
 405 hpDNA200, and (C) NR-hpDNA100 before and after hybridization ($[cDNA]=880$ nM). The
 406 fluorescence intensity decay curve of hpDNA was also presented for comparison. Samples were
 407 measured in 10 mM phosphate buffer (pH 7.5). (Lower panel) Fluorescence lifetime distributions
 408 of (D) NR-hpDNA400, (E) NR-hpDNA200, and (F) NR-hpDNA100 before and after
 409 hybridization obtained from MEM analysis. The fluorescence lifetime distribution of hpDNA
 410 was also included for comparison. Note the logarithmic lifetime axis.

411
 412
 413
 414

415 **Table 2.** Multi-exponential analysis of fluorescence intensity decays.

Samples	$\bar{\tau}$ /ns ^a	τ_i /ns ^b	f_i ^a	χ_R^2
hpDNA	3.87	3.92 ± 0.01	0.98	1.14
		0.47 ± 0.11	0.02	
hpDNA + cDNA	3.93	4.05 ± 0.02	0.94	1.08
		2.03 ± 0.07	0.06	
NR-hpDNA400	0.85	2.87 ± 0.15	0.08	1.11
		0.85 ± 0.03	0.59	
		0.35 ± 0.05	0.33	
NR-hpDNA400 + cDNA	1.40	3.93 ± 0.10	0.23	1.20
		1.05 ± 0.10	0.24	
		0.45 ± 0.03	0.53	
NR-hpDNA200	0.83	2.64 ± 0.18	0.11	1.18
		0.79 ± 0.04	0.57	
		0.31 ± 0.06	0.33	
NR-hpDNA200 + cDNA	2.71	3.96 ± 0.03	0.62	1.09
		1.15 ± 0.16	0.13	
		0.41 ± 0.05	0.25	
NR-hpDNA100	0.84	2.10 ± 0.21	0.10	1.13
		0.81 ± 0.05	0.51	
		0.33 ± 0.05	0.40	
NR-hpDNA100 + cDNA	3.02	3.95 ± 0.03	0.72	1.03
		1.25 ± 0.25	0.09	
		0.39 ± 0.05	0.20	

416 ^a The fluorescence decay was fitted to three exponentials plus scatter to take into account the
417 scatter effect caused by GNR. And the amplitude of scatter was excluded from the data analysis.

418 ^b The retrieved lifetimes are presented with three standard deviations as error.

419

420 **4. Conclusions**

421 In summary, a new GNR-based nanoprobe with potential for mRNA detection was developed by
422 functionalizing GNR with fluorophore labelled hairpin oligonucleotides. This nanoprobe was
423 found to be sensitive to a complementary oligonucleotide as indicated by significant changes in
424 fluorescence intensity and lifetime. Tuneable loading of hpDNA on GNR was achieved by
425 varying the molar ratio of hpDNA to GNR during the functionalization process. It was found that
426 the nanoprobe of higher hairpin coverage showed better performance in terms of sensitivity and
427 detection range from the steady-state fluorescence spectroscopy measurement. It was also found
428 that nanoprobe of the highest hairpin density captured the largest number of target strands, but
429 had relatively low hybridization ratio. Analysis by time-resolved fluorescence lifetime
430 spectroscopy revealed significant lifetime changes of the fluorophore after hpDNAs hybridized
431 with targets. It demonstrated that time-resolved fluorescence spectroscopy can be a powerful tool
432 in providing insight on the hybridization kinetics of the probe as well as the quenching effect of
433 GNR. We expect that this kind of GNR-based nanoprobe holds promise for mRNA detection
434 and subcellular imaging with the concomitant potential for a wide range of disease related
435 biomarker RNA analyses, including cancer diagnosis and prognosis.

436 **5. Acknowledgements**

437 We thank Dr J. Sutter, P. Yip and W. Li for assistance during the experimental work. This work
438 was funded by the BBSRC (BB/K013416/1). G.W. acknowledges financial support from the
439 China Scholarship Council (CSC).

440

441

442 **6. References**

- 443 1. C. E. Holt, S. L. Bullock, “Subcellular mRNA Localization in Animal Cells and Why It
444 Matters,” *Science* **326**, 1212–1216 (2009)
- 445 2. C. Eliscovich, A. R. Buxbaum, Z. B. Katz, R. H. Singer, “mRNA on the Move: The Road to
446 Its Biological Destiny,” *J. Biol. Chem.* **288**, 20361–20368 (2013)
- 447 3. R. W. Dirks, C. Molenaar, H. J. Tanke, “Methods for Visualizing RNA Processing and
448 Transport Pathways in Living Cells,” *Histochem. Cell Biol.* **115**, 3–11 (2000)
- 449 4. S. Tyagi, F. R. Kramer, “Molecular Beacons: Probes That Fluoresce upon Hybridization,”
450 *Nat. Biotechnol.* **14**, 303–308 (1996)
- 451 5. S. Tyagi, D. P. Bratu, F. R. Kramer, “Multicolor Molecular Beacons for Allele
452 Discrimination,” *Nat. Biotechnol.* **16**, 49–53 (1998)
- 453 6. T. Matsuo, “In Situ Visualization of Messenger RNA for Basic Fibroblast Growth Factor in
454 Living Cells,” *Biochim. Biophys. Acta* **1379**, 178–184 (1998)
- 455 7. D. L. Sokol, X. Zhang, P. Lu, A. M. Gewirtz, “Real Time Detection of DNA-RNA
456 Hybridization in Living Cells,” *Proc. Natl. Acad. Sci. U. S. A.* **95**, 11538–11543 (1998)
- 457 8. N. Nitin, P. J. Santangelo, G. Kim, S. Nie, G. Bao, “Peptide-Linked Molecular Beacons for
458 Efficient Delivery and Rapid mRNA Detection in Living Cells,” *Nucleic Acids Res.* **32**, e58
459 (2004)
- 460 9. C. D. Medley, T. J. Drake, J. M. Tomasini, R. J. Rogers, W. Tan, “Simultaneous Monitoring
461 of the Expression of Multiple Genes inside of Single Breast Carcinoma Cells,” *Anal. Chem.* **77**,
462 4713–4718 (2005)
- 463 10. B. Dubertret, M. Calame, A. J. Libchaber, “Single-Mismatch Detection Using Gold-
464 Quenched Fluorescent Oligonucleotides,” *Nat. Biotechnol.* **19**, 365–370 (2001)

- 465 11. Y. Zhang, D. J. S. Birch, Y. Chen, “Two-Photon Excited Surface Plasmon Enhanced Energy
466 Transfer between DAPI and Gold Nanoparticles: Opportunities in Intra-Cellular Imaging and
467 Sensing,” *Appl. Phys. Lett.* **99**, 103701 (2011)
- 468 12. C. Racknor, M. R. Singh, Y. Zhang, D. J. S. Birch, Y. Chen, “Energy Transfer between a
469 Biological Labelling Dye and Gold Nanorods,” *Methods Appl. Fluoresc.* **2**, 015002 (2013)
- 470 13. P. Gu, D. J. S. Birch, Y. Chen, “Dye-Doped Polystyrene-Coated Gold Nanorods: Towards
471 Wavelength Tuneable SPASER,” *Methods Appl. Fluoresc.* **2**, 024004 (2014)
- 472 14. S. Mayilo, M. A. Kloster, M. Wunderlich, A. Lutich, T. A. Klar, A. Nichtl, K. Kürzinger, F.
473 D. Stefani, J. Feldmann, “Long-Range Fluorescence Quenching by Gold Nanoparticles in a
474 Sandwich Immunoassay for Cardiac Troponin T,” *Nano Lett.* **9**, 4558–4563 (2009)
- 475 15. N. L. Rosi, D. A. Giljohann, C. S. Thaxton, A. K. R. Lytton-Jean, M. S. Han, C. A. Mirkin,
476 “Oligonucleotide-Modified Gold Nanoparticles for Intracellular Gene Regulation,” *Science* **312**,
477 1027–1030 (2006)
- 478 16. D. S. Seferos, D. A. Giljohann, H. D. Hill, A. E. Prigodich, C. A. Mirkin, “Nano-Flares:
479 Probes for Transfection and mRNA Detection in Living Cells,” *J. Am. Chem. Soc.* **129**, 15477–
480 15479 (2007)
- 481 17. A. E. Prigodich, D. S. Seferos, M. D. Massich, D. A. Giljohann, B. C. Lane, C. A. Mirkin,
482 “Nano-Flares for mRNA Regulation and Detection,” *ACS Nano* **3**, 2147–2152 (2009)
- 483 18. S. Song, Z. Liang, J. Zhang, L. Wang, G. Li, C. Fan, “Gold-Nanoparticle-Based Multicolor
484 Nanobeacons for Sequence-Specific DNA Analysis,” *Angew. Chemie - Int. Ed.* **48**, 8670–8674
485 (2009)

- 486 19. W. Pan, H. Yang, T. Zhang, Y. Li, N. Li, B. Tang, "Dual-Targeted Nanocarrier Based on
487 Cell Surface Receptor and Intracellular mRNA: An Effective Strategy for Cancer Cell Imaging
488 and Therapy," *Anal. Chem.* **85**, 6930–6935 (2013)
- 489 20. W. Pan, T. Zhang, H. Yang, W. Diao, N. Li, B. Tang, "Multiplexed Detection and Imaging
490 of Intracellular mRNAs Using a Four-Color Nanoprobe," *Anal. Chem.* **85**, 10581–10588 (2013)
- 491 21. A. Jayagopal, K. C. Halfpenny, J. W. Perez, D. W. Wright, "Hairpin DNA-Functionalized
492 Gold Colloids for the Imaging of mRNA in Live Cells," *J. Am. Chem. Soc.* **132**, 9789–9796
493 (2010)
- 494 22. S. R. Harry, D. J. Hicks, K. I. Amiri, D. W. Wright, "Hairpin DNA Coated Gold
495 Nanoparticles as Intracellular mRNA Probes for the Detection of Tyrosinase Gene Expression in
496 Melanoma Cells," *Chem. Commun. (Camb)*. **46**, 5557–5559 (2010)
- 497 23. C. J. Murphy, T. K. Sau, A. M. Gole, C. J. Orendorff, J. Gao, L. Gou, S. E. Hunyadi, T. Li,
498 "Anisotropic Metal Nanoparticles: Synthesis, Assembly, and Optical Applications," *J. Phys.*
499 *Chem. B* **109**, 13857–13870 (2005)
- 500 24. Y. Chen, J. A. Preece, R. E. Palmer, "Processing and Characterization of Gold Nanoparticles
501 for Use in Plasmon Probe Spectroscopy and Microscopy of Biosystems," *Ann. N. Y. Acad. Sci.*,
502 **1130**, 201–206 (2008)
- 503 25. R. Weissleder, "A Clearer Vision for in Vivo Imaging," *Nat. Biotechnol.* **19**, 316–317 (2001)
- 504 26. G. Boyd, Z. Yu, Y. Shen, "Photoinduced Luminescence from the Noble Metals and Its
505 Enhancement on Roughened Surfaces," *Phys. Rev. B* **33**, 7923–7936 (1986)
- 506 27. H. Wang, T. B. Huff, D. A. Zweifel, W. He, P. S. Low, A. Wei, J.-X. Cheng, "In Vitro and
507 in Vivo Two-Photon Luminescence Imaging of Single Gold Nanorods," *Proc. Natl. Acad. Sci.*
508 *U. S. A.* **102**, 15752–15756 (2005)

- 509 28. Y. Chen, Y. Zhang, D. J. S. Birch, A. S. Barnard, "Creation and Luminescence of Size-
510 Selected Gold Nanorods," *Nanoscale* **4**, 5017–5022 (2012)
- 511 29. Y. Zhang, J. Yu, D. J. S. Birch, Y. Chen, "Gold Nanorods for Fluorescence Lifetime Imaging
512 in Biology," *J. Biomed. Opt.* **15**, 020504 (2010)
- 513 30. A. Agarwal, S. W. Huang, M. O'Donnell, K. C. Day, M. Day, N. Kotov, S. Ashkenazi,
514 "Targeted Gold Nanorod Contrast Agent for Prostate Cancer Detection by Photoacoustic
515 Imaging," *J. Appl. Phys.* **102**, 064701 (2007)
- 516 31. C.-C. Chen, Y.-P. Lin, C.-W. Wang, H.-C. Tzeng, C.-H. Wu, Y.-C. Chen, C.-P. Chen, L.-C.
517 Chen, Y.-C. Wu, "DNA-Gold Nanorod Conjugates for Remote Control of Localized Gene
518 Expression by near Infrared Irradiation," *J. Am. Chem. Soc.* **128**, 3709–3715 (2006)
- 519 32. X. Huang, I. H. El-Sayed, W. Qian, M. A. El-Sayed, "Cancer Cell Imaging and Photothermal
520 Therapy in the near-Infrared Region by Using Gold Nanorods," *J. Am. Chem. Soc.* **128**, 2115–
521 2120 (2006)
- 522 33. Y. Zhang, G. Wei, J. Yu, D. Birch, Y. Chen, "Surface Plasmon Enhanced Energy Transfer
523 between Gold Nanorods and Fluorophores: Application to Endocytosis Study and RNA
524 Detection," *Faraday Discuss.* **178**, 383-394 (2015)
- 525 34. B. Nikoobakht, M. A. El-Sayed, "Preparation and Growth Mechanism of Gold Nanorods
526 (NRs) Using Seed-Mediated Growth Method," *Chem. Mater.* **15**, 1957–1962 (2003)
- 527 35. T. K.; Sau, C. J. Murphy, "Seeded High Yield Synthesis of Short Au Nanorods in Aqueous
528 Solution," *Langmuir* **20**, 6414–6420 (2004)
- 529 36. A. Wijaya, K. Hamad-Schifferli, "Ligand Customization and DNA Functionalization of Gold
530 Nanorods via Round-Trip Phase Transfer Ligand Exchange," *Langmuir* **24**, 9966–9969 (2008)

531 37. C. J. Orendorff, C. J. Murphy, “Quantitation of Metal Content in the Silver-Assisted Growth
532 of Gold Nanorods,” *J. Phys. Chem. B* **110**, 3990–3994 (2006)

533 38. L. M. Demers, C. A. Mirkin, R. C. Mucic, R. A. Reynolds, R. L. Letsinger, R. Elghanian, G.
534 Viswanadham, “A Fluorescence-Based Method for Determining the Surface Coverage and
535 Hybridization Efficiency of Thiol-Capped Oligonucleotides Bound to Gold Thin Films and
536 Nanoparticles,” *Anal. Chem.* **72**, 5535–5541 (2000)

537 39. K. A. Brown, S. Park, K. Hamad-Schifferli, “Nucleotide–Surface Interactions in DNA-
538 Modified Au–Nanoparticle Conjugates: Sequence Effects on Reactivity and Hybridization,” *J.*
539 *Phys. Chem. C* **112**, 7517–7521 (2008)

540 40. S. J. Hurst, A. K. R. Lytton-Jean, C. A. Mirkin, “Maximizing DNA Loading on a Range of
541 Gold Nanoparticle Sizes” *Anal. Chem.* **78**, 8313–8318 (2006)

542 41. A. Wijaya, S. B. Schaffer, I. G. Pallares, K. Hamad-Schifferli, “Selective Release of Multiple
543 DNA Oligonucleotides from Gold Nanorods,” *ACS Nano* **3**, 80–86 (2009)

544 42. J. Brochon, “Maximum Entropy Method of Data Analysis in Time-Resolved Spectroscopy,”
545 *Methods Enzymol.* **240**, 262–311 (1994)

546 43. A. M. Alkilany, P. K. Nagaria, C. R. Hexel, T. J. Shaw, C. J. Murphy, M. D. Wyatt, “Cellular
547 Uptake and Cytotoxicity of Gold Nanorods: Molecular Origin of Cytotoxicity and Surface
548 Effects,” *Small* **5**, 701–708 (2009)

549 44. Y. Zhang, D. Xu, W. Li, J. Yu, Y. Chen, “Effect of Size, Shape, and Surface Modification on
550 Cytotoxicity of Gold Nanoparticles to Human HEp-2 and Canine MDCK Cells,” *J. Nanomater.*
551 **2012**, 1–7 (2012)

552 45. V. Sharma, K. Park, M. Srinivasarao, “Shape Separation of Gold Nanorods Using
553 Centrifugation,” *Proc. Natl. Acad. Sci. U. S. A.* **106**, 4981–4985 (2009)

554 46. H. D. Hill, J. E. Millstone, M. J. Banholzer, C. A. Mirkin, “The Role Radius of Curvature
555 Plays in Thiolated Oligonucleotide Loading on Gold Nanoparticles,” *ACS Nano* **3**, 418–424
556 (2009)

557 47. S. Tyagi, S. A. E. Marras, J. A. M. Vet, F. R. Kramer, “Molecular Beacons : Hybridization
558 Probes for Detection of Nucleic Acids in Homogeneous Solutions,” in *Nonradioactive Analysis*
559 of Biomolecules, 606-616, Ed. C. Kessler, Springer, (2000) DOI 10.1007/978-3-642-57206-7_53

560 48. B. G. Moreira, Y. You, M. A. Behlke, R. Owczarzy, “Effects of Fluorescent Dyes,
561 Quenchers, and Dangling Ends on DNA Duplex Stability,” *Biochem. Biophys. Res. Commun.*
562 **327**, 473–484 (2005)

563 49. A. W. Peterson, R. J. Heaton, R. M. Georgiadis, “The Effect of Surface Probe Density on
564 DNA Hybridization,” *Nucleic Acids Res.* **29**, 5163–5168 (2001)

565 50. K. B. Cederquist, C. D. Keating, “Hybridization Efficiency of Molecular Beacons Bound to
566 Gold Nanowires: Effect of Surface Coverage and Target Length,” *Langmuir* **26**, 18273–18280
567 (2010)

568 51. R. Levicky, T. M. Herne, M. J. Tarlov, S. K. Satija, “Using Self-Assembly To Control the
569 Structure of DNA Monolayers on Gold: A Neutron Reflectivity Study,” *J. Am. Chem. Soc.* **120**,
570 9787–9792 (1998)

571 52. A. O. Crockett, C. T. Wittwer, “Fluorescein-Labeled Oligonucleotides for Real-Time Pcr:
572 Using the Inherent Quenching of Deoxyguanosine Nucleotides,” *Anal. Biochem.* **290**, 89–97
573 (2001)

574 53. J. R. Unruh, G. Gokulrangan, G. S. Wilson, C. K. Johnson, “Fluorescence Properties of
575 Fluorescein, Tetramethylrhodamine and Texas Red Linked to a DNA Aptamer,” *Photochem.*
576 *Photobiol.* **81**, 682–690 (2005)

577 54. T. Heinlein, J.-P. Knemeyer, O. Piestert, M. Sauer, “Photoinduced Electron Transfer between
578 Fluorescent Dyes and Guanosine Residues in DNA-Hairpins,” *J. Phys. Chem. B* **107**, 7957–7964
579 (2003)

580 55. G. Wei, D. Simionesie, J. Sefcik, J. U. Sutter, Q. Xue, J. Yu, J. Wang, D. J. S. Birch, Y.
581 Chen, “Revealing the Photophysics of Gold-Nanobeacons via Time-Resolved Fluorescence
582 Spectroscopy,” *Opt. Lett.* **40**, 5738-5741 (2015)

583

584 **Caption List**

585 **Scheme 1.** Schematic illustration of hairpin DNA functionalized GNR for mRNA detection.

586 **Figure 1.** (a) TEM image of the gold nanorods. The scale bar is 200 nm; (b) Extinction spectra
587 of GNR made with CTAB and GNRs with surface modifications of MHA and hpDNA-FAM.
588 The NR-CTAB was suspended in distilled water, while NR-MHA and NR-hpDNA-FAM were
589 suspended in 1×TBE (pH 8.3) and 10 mM phosphate buffer (pH 7.5), respectively.

590 **Figure 2.** A correlation between surface loading of hpDNA on each GNR and molar ratio of
591 hpDNA to GNR in the synthesis process. Error bars are one standard deviation from three
592 measurements.

593 **Figure 3.** Kinetic fluorescence measurements of the nanoprobe upon hybridization. The
594 concentrations of NR-hpDNA and cDNA were 0.22 and 880 nM, respectively. Excitation
595 wavelength: 490 nm; fluorescence wavelength: 517 nm.

596 **Figure 4.** Dose response of the nanoprobe (0.22 nM) with different surface packing densities of
597 hpDNA. The concentrations of perfectly complementary DNA were 0, 1, 5, 10, 20, 30, 40, 50,
598 80, 100, 200 and 300 nM. Excitation wavelength: 485 nm; emission peak: 517 nm.

599 **Figure 5.** (Upper panel) Fluorescence intensity decay curves of (A) NR-hpDNA400, (B) NR-
600 hpDNA200, and (C) NR-hpDNA100 before and after hybridization ([cDNA]=880 nM). The
601 fluorescence intensity decay curve of hpDNA was also presented for comparison. Samples were
602 measured in 10 mM phosphate buffer (pH 7.5). (Lower panel) Fluorescence lifetime distributions
603 of (D) NR-hpDNA400, (E) NR-hpDNA200, and (F) NR-hpDNA100 before and after

604 hybridization obtained from MEM analysis. The fluorescence lifetime distribution of hpDNA
605 was also included for comparison. Note the logarithmic lifetime axis.

606 **Table 1.** Hybridization efficiency of NR-hpDNA nanoprobe with different probe surface
607 packing densities.

608 **Table 2.** Multi-exponential analysis of fluorescence intensity decays.

609

610

611

612